

1                   **VISCOELASTICITY MODELLING OF ASPHALT MASTICS UNDER PERMANENT**  
2                   **DEFORMATION THROUGH THE USE OF FRACTIONAL CALCULUS**

3  
4 M. Lagos-Varas<sup>a,b,\*</sup>, D. Movilla-Quesada<sup>b,c</sup>, A.C. Raposeiras<sup>b,d</sup>, D. Castro-Fresno<sup>a</sup>, O. Muñoz-Cáceres<sup>a,b</sup>,  
5 V. C. Andrés-Valeri<sup>b</sup>, M.A. Rodríguez-Esteban<sup>c</sup>  
6

7 <sup>a</sup> GITECO Research Group, University of Cantabria, Av. Los Castros, 39005 Santander, Spain.

8 <sup>b</sup> Gi<sup>2</sup>V Research Group, Institute of Civil Engineering, Faculty of Engineering Sciences, University  
9 Austral of Chile, Valdivia, Chile.

10 <sup>c</sup> Departamento de Construcción y Agronomía, Escuela Politécnica Superior de Zamora, Universidad de  
11 Salamanca, 49029 Zamora, España.

12 <sup>d</sup> Departamento de Ingeniería Mecánica, Escuela Politécnica Superior de Zamora, Universidad de  
13 Salamanca, 49029 Zamora, España.  
14

15 **ABSTRACT**

16 This study focuses on the mechanical behaviour of asphalt mastic composed of filler particles bonded with  
17 an asphalt bitumens. Asphalt mastics are viscoelastic composite materials widely used in the construction  
18 of pavement layers. The mechanical properties and the influence of the fillers on the filler/bitumen (f/b)  
19 matrix is one of the main areas of current research. In particular, the elastic determination of fillers for  
20 mechanical testing in asphalt mastic is relevant to understand permanent deformation caused by  
21 temperature variations caused by seasonal changes and vehicular traffic loads. In this sense, this research  
22 proposes a new methodology for rheological characterization of the elastic properties of the filler  $\xi_2$  and  
23 elastic-viscous properties of the asphalt bitumen,  $\xi_1$  and  $\eta$ , respectively, complementing the existing  
24 designs of asphalt mixture. The proposed methodology allows for identification of the influence of non-  
25 conventional fillers in the behavior of the asphalt mastic for the different recovery cycles of the Multiple  
26 Stress Creep Recovery (MSCR) and determination of new rheological parameters for the compression of  
27 the recovery phenomena and the elastic capacity of the type of filler and weight of the base bitumen. The  
28 results obtained show a greater adjustment to the experimental curves in determining the elastic modulus  
29 in each cycle for the hydrated lime and fly ash fillers with different filler/bitumen ratios. In particular, the  
30 proposed model for bituminous mastics achieves a strong fit with the experimental curves by empirically  
31 reducing the quadratic error ( $R^2 = 0.99$ ) and managing to differentiate the elastic capacity  $\xi_2$  of each filler  
32 and its effect with increasing concentration. For example, it establishes that the Hydrated lime filler (HL)  
33 acquires an average Young's modulus of 0.005 MPa, being 99.31% more elastic than Fly ash filler (FA)  
34 for a load of 3.2 kPa at a 1.25 f/b ratio. In addition, the new model can be used to modify bitumen properties  
35 to design optimized and stronger asphalt mixtures.  
36

37 **Keywords:** Rheology, Permanent deformation, asphalt mastic, filler/bitumen, creep-recovery, hydrated  
38 lime, fly ash  
39  
40

## 1. INTRODUCTION

The asphalt mixture is a composite of aggregates (coarse and fine aggregates), asphalt bitumen, air and possibly additive and modifying components [1,2]. These materials form a system in which the aggregate is enveloped by a continuous film of asphalt bitumen [3]. The filler, whose particle size is less than 0.063 mm (according to EN 13043), is trapped by the asphalt bitumen, forming the asphalt mastic, which favours the agglomeration of the larger aggregates and influencing the properties of hot mix asphalt (HMA) [4].

In the last decades, the rheological study of the filler/bitumen (f/b) interaction has been relevant to know the properties that most influence the asphalt pavement, allowing the study of failures such as rutting and irregularities in the road surface, which cause premature deterioration of the pavement and a reduction in traffic comfort and safety [5,6]. The rheological analysis of the materials that compose the asphalt mixtures allows demonstrating, through the f/b interface, that the mastic has a high rutting resistance, even allowing improving the skid resistance, reducing the rolling noise and increasing the life cycle of the pavement.

The filler plays a fundamental role in this regard, since, due to its high specific surface area, it can withstand the stresses caused by internal friction or by contact between particles [7]. The characteristics of the filler, such as morphology, composition, friction between particles, behaviour under humidity and temperature, generate physicochemical properties that develop a high degree of interaction with the bitumen, improving the mechanical behaviour of the mastic. The main fillers used as the mineral skeleton of the mastic are limes [8], fly ash [9], hydrated lime [10], slags [11], and others.

However, the most commonly used filler is limestone, due to the positive impact it has on the durability of asphalt mixtures, reducing the appearance of cracks caused by the effect of water and temperature variations.

The limestone filler (denoted as "L") increases the stiffness of the asphalt mixture and reactivates the asphalt bitumen, improving the adhesiveness between the aggregate-bitumen system [12]. Similarly, the use of hydrated lime (referred to as "HL") as a filler in asphalt mastics increases the mechanical strength of the asphalt mixture, minimizing the appearance of cracks [13], ageing and increasing the stiffness of the mastic [14]. In addition, when the HL has a degree of compatibility with the asphalt bitumen, a molecular layer is absorbed that positively affects the rheology of the mastic at high temperatures and to a greater degree if compared with inert fillers [15]. Likewise, HL filler improves the adhesiveness between the bitumen and the aggregate surface in an asphalt mixture, due to the water-insoluble salts generated by the precipitation of calcium ions, which prevents premature separation of the aggregate-bitumen interface [16].

On the other hand, results obtained in previous research have shown that the use of construction and demolition wastes (CDWs) and/or industrial and commercial by-products in asphalt mixtures is a good alternative from a sustainable (social, economic and environmental) point of view [17]. For example, fly ash (FA) is an industrial waste widely used as an environmentally friendly filler in asphalt mixtures. These fillers provide greater elasticity compared to limestone filler, improving the flexibility of the asphalt pavement. In addition, they have a significant impact on the viscosity and rheological properties of asphalt mastics, thus affecting the final strengths of asphalt mixtures [18].

According to the Marshall parameters for dense asphalt mixtures, the addition (up to 4%) of FA as a replacement for HL results in a 7.5% reduction in the optimum asphalt bitumen content, which minimizes the production cost of large-scale asphalt mixtures [19].

In 2017, researchers Li *et al.* [20] evaluated the thickness of the absorbing film between the filler and the asphalt bitumen, as it is an indicator of the physicochemical interaction and rheological properties of the asphalt mastic. The results showed that the FA filler has a thicker absorbed film compared to that of the HL filler, with those generated by L having a thinner film.

The asphalt bitumen has a rheology that is determined by viscoelastic behaviour, to which elastic and viscous deformations are assigned [21,22]. Currently, the study of these deformations analyzes using its capacity to transform elastic-viscous states, under static and dynamic loads [23,24]. The mechanical characterization of the asphalt bitumen is achieved from classical methodologies of linear viscoelasticity, or techniques based on the damage resistance characterization. Classical methodologies allow the determination of softening, penetration points, brittleness, viscosity, among others, at a single temperature point [25]. However, current methods are based on the total deformation resistance and its relationship between the elastic and viscous parts of the asphalt bitumen [26].

The SUPERPAVE methodology allows the analysis of the rheological behaviour of asphalt bitumen and asphalt mixtures for a wide range of temperatures and loading frequencies [27]. In particular, this methodology establishes the parameter " $|G^*|/\sin(\delta)$ " for the study of permanent deformations at elevated temperatures, determining a limit of the vulnerability of the asphalt bitumen to rutting failures [28]. However, several authors have stated that this parameter only considers linear viscoelastic (LVE) rheology [29], which does not effectively represent permanent deformation, since in asphalt mixtures this anomaly occurs in a nonlinear viscoelastic range. Thus, to identify a plasticity index that describes the rutting damage

caused by the trajectory of the tire in the asphalt mixture, the Federal Highway Administration (FHWA) proposed to study the performance of asphalt bitumens for intermediate-high temperatures using the multiple stress creep recovery test (MSCR) [30].

The MSCR test generates stresses from multiple creep and recovery phenomena by evaluating the non-recoverable creep compliance ( $J_{nr}$ ) [31] and the mean percentage recovery ( $R$ ), which show the potential rutting rate and elasticity of the asphalt bitumen, respectively [32]. Creep and recovery phenomena generate in static cycles with controlled times [33]. Creep occurs in the process of specimen loading, which generate recoverable and non-recoverable strain states for non-linear viscoelastic deformations [1]. Subsequently, the recovery phenomenon details the capacity of the asphalt bitumen to redeem the deformations obtained in the creep process, determining the degree of plasticization in each cycle [34]. In addition, these parameters can reflect the rutting resistance of the asphalt mastic, where the load of 3.2 kPa is the one that generates a more accurate correlation to the permanent deformations in asphalt mixtures [35].

However, this methodology does not quantify the elastic capacity or Young's modulus of the type of filler used, nor does it allow evaluating a degree of softening of the f/b, as a measure of viscoelastic transition for a given temperature. Therefore, the application of a rheological model proposes, which establishes a set of springs and fractional dampers, representing a mineral aggregate particle (filler) with an agglomeration of the asphalt bitumen, to understand the rheology exhibited by the asphalt mastic, filler and bitumen jointly and/or independently. In this sense, the use of the mathematical equations of the proposed model allows detailing the viscoelastic transitions of the asphalt bitumen, quantifying the elastic capacity of the filler used and its relationship with the f/b dosage by means of the MSCR recovery phenomena [36].

The objective of this study is to establish the influence of fillers made up of HL, FA and L on the viscoelastic behaviour of asphalt mastic based on a rheological characterization of the filler/bitumen matrix by means of different loading rate, temperature, and dosage conditions. The study provides a new methodology to characterize the recovery phenomenon for each cycle of the MSCR test, knowing that the proposed model determines the degree of viscoelasticity and mechanical properties of the materials [1,36]. The application of the model establishes the Young's modulus of HL, FA and L for different dosage percentages (f/b 0.50, 0.75, 1.00 and 1.25) with respect to the weight of the base asphalt bitumen.

## 2. MATERIALS AND METHODS

### 2.1. Asphalt bitumen and mastic

In this study, the conventional asphalt bitumen B50/70 was used, whose classic mechanical properties summarized in Table 1 with the essential characteristics and specifications.

**Table 1.** Characteristics of the asphalt bitumen B50/70

Properties	Standard	Results
Penetration at 25°C (0,1 mm)	EN 1426	57.00
Softening point (°C)	EN 1427	51.60
Frass breaking point (°C)	EN 12593	-13.00
Density (g/cm <sup>3</sup> )	EN 15326	1.035

The fillers used for the manufacture of asphalt mastics are: HL, FA and L (Figure 1). The aggregates use mostly used in wearing courses due to their mechanical properties, guaranteeing the necessary surface texture for some time. In addition, it is known that HL and L fillers possess a high content of calcium oxide (CaO) at 90.67% and 88.65%, respectively [37,38]. Leaving other main components such as silicon dioxide (SiO<sub>2</sub>) and magnesium oxide (MgO) in second place [37]. FA have high SiO<sub>2</sub> content between 43.53-60.31% depending on their nature [39], in addition to other compounds such as CaO and Al<sub>2</sub>O<sub>3</sub> to a lesser extent [40].

The characterization of the basic properties (see Table 2) of the fillers used based on the determination of particle density by the pycnometer method according to EN 1097-7. In addition, the content of Rigden voids (RV) was calculated based on the EN 1097- 4 procedure from the density obtained.



**Figure 1.** The fillers used sifted through an N°200 (0.08 mm) sieve. a) HL; b) FA; c) L

147

**Table 2.** Physical and geometric properties of the fillers

Properties	Hydrated lime (HL)	Fly ash (FA)	Limestone (L)
Density (g/cm <sup>3</sup> )	1.959	2.450	2.725
Rigiden voids (%)	76	73	74
Granulometric analysis (%)			
Sieve (mm)	% Passed Through		
0.063 mm	98.65	97.65	81.28
0.050 mm	76.90	72.77	39.81
0.040 mm	63.94	62.69	24.42
0.032 mm	46.21	37.65	7.86
0.020 mm	21.58	11.60	0.17

148

149

150

151

152

153

The manufacturing process of the asphalt mastics is carried out by mixing the base bitumen type B50/70 with the fillers of HL, FA and L, independently. Several samples are generated based on the filler/bitumen (f/b) dosage for each of the fillers mentioned. The f/b ratios in a mass of base bitumen are 0.50, 0.75, 1.00 and 1.25. Additionally, B50/70 base bitumen samples prepared for the analysis of reference samples.

154

155

156

157

158

159

160

As for the fabrication of the samples, the B50/70 base bitumen was heated in an oven at 153°C for 2 hours until medium aging was achieved in an asphalt mix (Figure 2). In addition, the fillers used were heated at a temperature of 170°C for four hours to create mastic samples under the same conditions as those obtained in an asphalt mix. The mastic samples were not aged using the Rolling Thin Film Oven Test (RTFOT) as it is indicated in the AASHTO M 332 since the objective is to simulate the recovery curves of asphalt mastics for the classification of filler elasticity and bitumen viscoelasticity, and that these mastics are equivalent to those of asphalt mixtures manufactured in the laboratory.

161

162

163

164

165

166

167

168

169

170

Subsequently, a portion of the dosed mass of the asphalt bitumen was deposited in a mixer homogenizer at 153-154°C. The previously prepared fillers of HL, FA and L are added individually to the base bitumen for each dosage slowly for better homogenization. The speed and time of manufacture vary in prior art studies depending on digestion and/or air removal in homogenization (5-30 min and 500-4500 rpm). The HL charge with the highest dosage (f/b=1.25) was used as a reference in digestion time and speed because it has the highest mass concentration. Therefore, a manufacturing process at 1500 rpm in about 10-15 min was defined, which is within the actual process. Finally, the homogeneous mixture is deposited in the 8 and 25mm molds standardized for testing in the dynamic shear rheometer (DSR), obtaining 13 different types of asphalt mastic samples.

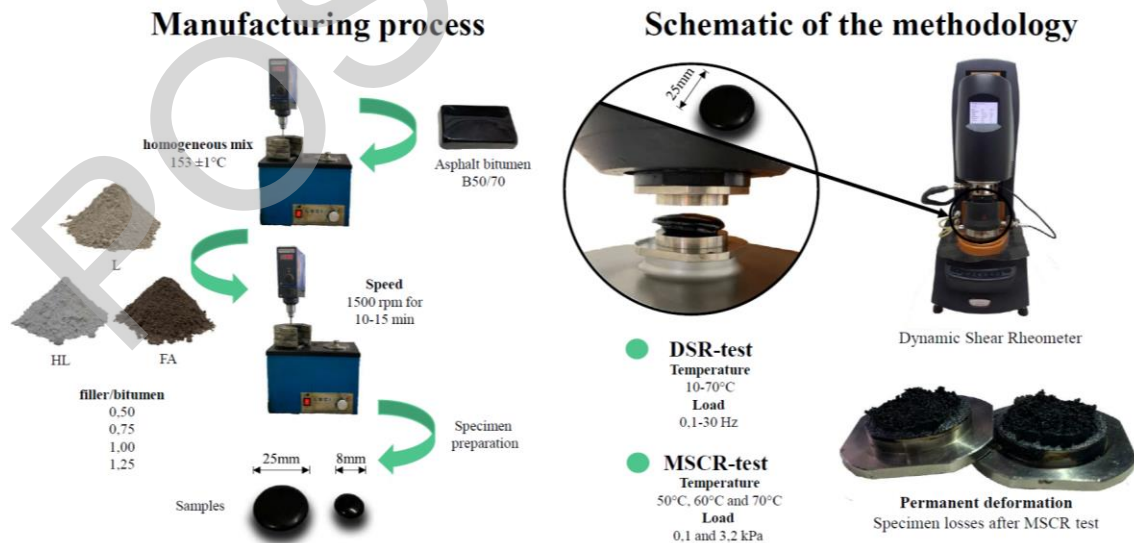


**Figure 2.** Schematic of the manufacture and methodology for determining the rheological properties of asphalt mastics.

171

172

## 2.2. Mechanical properties of linear viscoelasticity

173 The linear viscoelastic properties of asphalt bitumen and mastics are determined by the DSR-test  
174 methodology, applying the master curve fitting for the complex modulus  $|G^*|$  and angle of phase  $\delta$  [41,42].

175 The values of the  $|G^*|$  vector and angle  $\delta$  are obtained using two parallel plates of known geometry. El  
176 The temperature sweep of the test extends from 10°C to 70°C. A 25 mm parallel plate is used for the 30 to  
177 70°C temperature range, and an 8 mm parallel plate used for the 10 to 30°C range. The 30°C temperature  
178 averaged for the two ranges with a difference of less than 5%. The oscillating model of the test is performed  
179 for 10 frequencies in a range from 0.1 to 30 Hz, with a sinusoidal displacement of 0.1% strain.

180 The master curves used to understand the susceptibility between temperature and load frequency  
181 variables in two dimensions. In the present study, a master curve fit by time-temperature superposition [43]  
182 is used for the values of  $|G^*|$  and  $\delta$ , from the test frequencies and temperatures (10 to 70°C), converging to  
183 a single curve approximated by the sigmoidal function (see Eq. (1)).  
184

$$\log(G^*) = \alpha + \frac{\lambda}{1 + e^{\varphi - \gamma \cdot \log(\omega_r)}} \quad (1)$$

185  
186 Where,  $\alpha$  is the lower asymptote,  $\lambda$  is the difference between the upper and lower asymptote values,  
187  $\varphi$  is the inflexion point,  $\gamma$  is the slope, and  $\omega_r$  is the reduced frequency.

188 An index ( $I_{mastic}$ ) has been defined to provide an interpretation of the results and quantify the  
189 variation of the mass increase on the fillers. The variable  $I_{mastic}$  (see Eq. (2)) is only a proposed indicator to  
190 obtain the ranges of possible values of  $G^*$  caused by the type of filler for  $\omega_r$ . The objective is only to  
191 calculate the maximum and minimum value of  $G^*$  when varying the concentration, with respect to its lower  
192 dosage. The theoretical foundation is based solely on the time-temperature superposition principle, defined  
193 by Eq. (1) for the extreme concentrations (f/b 0.50 and 1.25). The difference of the area under the curve is  
194 calculated by means of an integral defined and calculated with MATLAB© for each curve, obtaining a  
195 stiffness domain by type of filler used.  
196

$$I_{mastic} = \int_{\alpha}^{\alpha+\lambda} \left[ \log \frac{G^*(\omega_r, f/b=1.25)}{G^*(\omega_r, f/b=0.50)} - \log G^*(\omega_r, f/b=0.50) \right] d\omega_r \quad (2)$$

197  
198 Where  $G^*$  is the complex modulus,  $\omega_r$  is the reduced frequency for each dosage f/b between the integral  
199 limits of the sigmoidal curve.  
200

### 201 2.3. Damage resistance characterization mechanical properties

#### 202 2.3.1. MSCR test

203 In this study, the MSCR test performed for the base bitumen and asphalt mastics at a test  
204 temperature of 50°C, 60°C and 70°C by performing 20 continuous loading and unloading cycles with 25  
205 mm diameter plate on the DSR (AASHTO T 350). The load is set for a torque of 0.1 kPa to condition the  
206 specimens and then at 3.2 kPa to cause damage to the specimen.

207 The creep phenomenon set with a time of 1 s and the recovery extended 9 s. The two parameters  
208 of the MSCR test are non-recoverable compliance ( $J_{nr}$ ) and percentage recovery (R) (AASHTO M 332).  
209 The above parameters establish criteria for evaluating yield strain and recovery capability of samples using  
210 Eqs. (3) and (4), respectively:  
211

$$J_{nr\sigma}(1/kPa) = \frac{1}{10} \sum_{i=1}^{10} \frac{\gamma_{n_i} - \gamma_{0_i}}{\sigma} \quad (3)$$

$$R_{\sigma}(\%) = \frac{1}{10} \sum_{n=1}^{10} \frac{\gamma_{p_i} - \gamma_{n_i}}{\gamma_{p_i} - \gamma_{0_i}} \quad (4)$$

212  
213 where  $\gamma_0$  represents the shear stress at the beginning of the cycle,  $\gamma_p$  is the point of most significant  
214 deformation after 1 s of load,  $\gamma_n$  represents the non-recoverable stress at the end of the first cycle, and  $\tau$   
215 represents the yield stress in each period. Thus, four parameters are obtained ( $R_{0.1}$ ,  $J_{nr0.1}$ ,  $R_{3.2}$ , and  $J_{nr3.2}$ )  
216 which indicate the standard mean of each phenomenon for the two load quantities.  
217

#### 218 2.4. Rheological models for bitumen and asphalt mastic

219 The rheological simulation of the MSCR based on a mechanical representation of the bitumen and  
220 mastic asphalt (Figure 3), demonstrated for the viscoelastic deformations of the filler/bitumen system. The  
221 model defines the elastic property of the filler utilizing the variable  $\xi_2$  (kPa), representing Young's modulus

222 for each type of filler and its relationship with the dosage  $f/b$ . In the case of the asphalt bitumen, the  
 223 variables  $\xi_i$  (kPa) and  $\eta$  (kPa·s) established for the elastic and viscous representation of the B50/70 base  
 224 bitumen defined for each temperature and test load.

225 The Riemann-Liouville integral and fractional derivative of a function are defined as follows  $f(t)$ , in  
 226 the Eqs. (5) and (6) respectively, to obtain the differential equation of the model [44]:  
 227

$$D_t^{-\alpha} f(t) = \frac{1}{\Gamma(\alpha)} \int_0^t (t-u)^{\alpha-1} f(u) du, \quad \alpha > 0, \quad (5)$$

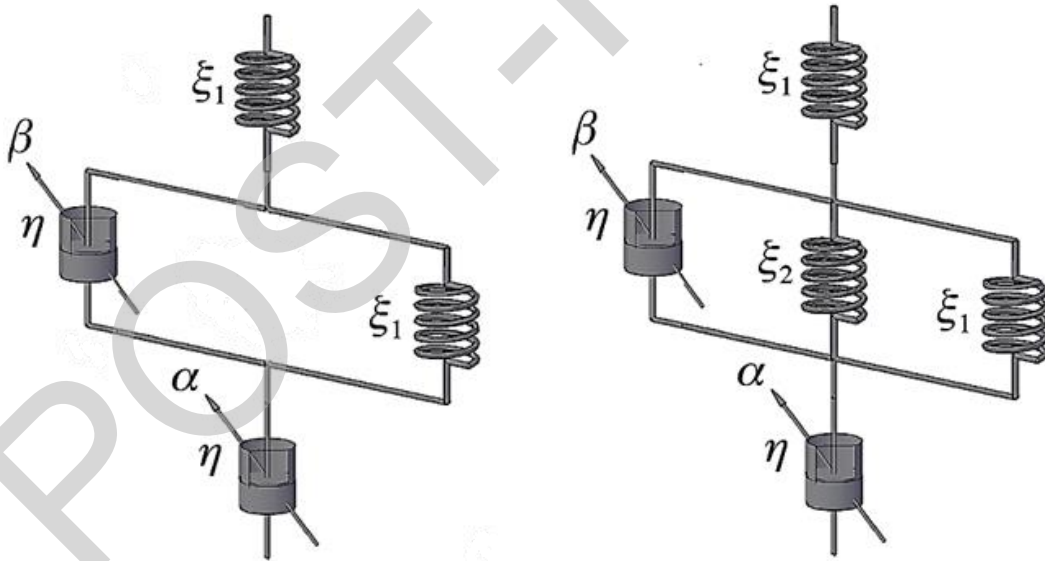
$$D_t^{\alpha} f(t) = D^n D^{\alpha-n} f(t) = \frac{1}{\Gamma(n-\alpha)} \frac{d^n}{dt^n} \int_0^t \frac{f(u)}{(t-u)^{\alpha-n+1}} du, \quad \alpha > 0, \quad (6)$$

228 Where  $n$  is a positive number,  $n-1 \leq \alpha < n$ ,  $t$  is time and  $\Gamma(\cdot)$  is the Gamma function. Particularly, when  
 229  $\alpha=n$ , then  $D_t^{\alpha} f(t) = d^n/Dt^n f(t)$ .

230 The differential equation governing the model for asphalt mastics is obtained after applying the above  
 231 definition, based on the use of fractional calculus as it is shown in Eq. (7). The mathematical development  
 232 achieved by adding the unit deformations of the mechanical elements. With this, the fractional derivatives  
 233  $\alpha, \beta, \gamma$  are established, which have a range of possible values between 0 and 1, to satisfy the classical  
 234 equations of the Maxwell and Kelvin-Voigt models [45]. By substituting and transforming the derivatives  
 235 algebraically [1].  
 236  
 237

$$D_t^{\alpha+\beta} \epsilon(t) + \frac{M}{\eta} D_t^{\alpha} \epsilon(t) = \frac{1}{\xi_1} D_t^{\beta+\gamma} \sigma(t) + \frac{1}{\eta} D_t^{\beta} \sigma(t) + \frac{1}{\eta} D_t^{\alpha} \sigma(t) + \frac{M}{\xi_1 \eta} D_t^{\gamma} \sigma(t) + \frac{M}{\eta^2} \sigma(t) \quad (7)$$

238 Where  $\epsilon(t)$  is the strain,  $\sigma(t)$  is the stress,  $M = \xi_1 + \xi_2$  and  $D_t^{\alpha}, D_t^{\beta}$  and  $D_t^{\gamma}$  are the fractional derivatives  
 239 with respect to time  $t$ .  
 240  
 241



242 **Figure 3.** Schematic diagram of the rheological models. a) Asphalt bitumen; b) Asphalt mastic

243 The recovery phenomenon begins when the initial 1s MSCR-test stress is released, giving rise to  
 244 a function that depends on time and material type. To describe this process, it is necessary to consider Eq.  
 245 (7) by eliminating the concept of initial stress  $\sigma_0=0$  resulting in the following definition [1]:  
 246

$$\hat{\epsilon} \left[ s^{\alpha+\beta} - \sum_{k=0}^{m-1} s^{\beta+\alpha-k-1} \epsilon^k(0) + \frac{M}{\eta} s^{\alpha} - \sum_{k=0}^{m-1} s^{\beta-k-1} \epsilon^k(0) \right] = 0 \quad (8)$$

247

248 Where  $\alpha$  and  $\beta$  values between  $m-1$  and  $m$ ,  $m$  is the positive number closest to the value of  $\alpha$  and  
 249  $\beta$ . Having said this, and by means of the Mittag-Leffler ( $E_q$ ) [46] with the argument  $-at^\alpha$ , the following  
 250 Laplace transform is defined:  
 251

$$L\{E_\alpha[-at^\alpha]\} = L\left\{\sum_{k=0}^{\infty} \frac{(-at^\alpha)^k}{\Gamma(k\alpha + 1)}\right\} = L\left\{\sum_{k=0}^{\infty} \frac{(-a)^k t^{k\alpha}}{\Gamma(k\alpha + 1)}\right\} = \frac{s^\alpha}{s(s^\alpha - a)} \quad \alpha > 0 \quad (9)$$

252 After applying the above definition, the recovery function of the bitumen and asphalt mastic for the MSCR  
 253 test is obtained in fractional form in Eqs. (10) and (11), respectively:  
 254  
 255

$$R_{Bitumen}(t) = \epsilon_M^0(0) \sum_{k=0}^{\infty} \frac{\left(-\frac{\xi_1}{\eta} t^\beta\right)^k}{\Gamma(1 + \beta k)} + \epsilon_\infty^0(0), \quad (10)$$

$$R_{Mastic}(t) = \epsilon_M^0(0) \sum_{k=0}^{\infty} \frac{\left(-\frac{M}{\eta} t^\beta\right)^k}{\Gamma(1 + \beta k)} + \epsilon_\infty^0(0), \quad (11)$$

256 where  $R_{Mastic}(t)$  is the recovery strain for asphalt mastic,  $R_{Bitumen}(t)$  is the recovery strain for asphalt  
 257 bitumen,  $\Gamma(\cdot)$  is the Gamma function,  $\epsilon_\infty^0(0)$  is the adjustment factor of the Maxwell's model [47], and  
 258  $\epsilon_M^0(0)$  is the adjustment factor of the parallel system and Mittag-Leffler infinite series, which depends on  
 259 the parameter and which describes the viscoelastic transformation process  $M = \xi_1 + \xi_2$ , which is the elastic  
 260 capacity of the bituminous mastic.  
 261

### 262 3. RESULTS AND DISCUSSION

#### 263 3.1. Analysis of the dynamic modulus $|G^*|$ and phase angle $\delta$

264 Figure 4 shows the master curves  $|G^*|$  and the variation of the offset angle of the base bitumen and the  
 265 asphalt mastics.  
 266

267 The results show that the mastics in their different f/b ratios generate a band of use characteristic of  
 268 the stiffness capacity of the filler type. In particular, an increase in stiffness obtained for the three types of  
 269 mastics (HL, FA and L) with increasing f/b concentration. For low temperatures or high reduced  
 270 frequencies  $\omega_r$ , no major differences between the filler types observed, reaching an average stiffness of 109  
 271 Pa. On the contrary, for high temperatures or low reduced frequencies  $\omega_r$ , differences are observed in the  
 272 samples due to the thermal susceptibility and the amount of mass per unit volume of the asphalt bitumen.

273 Samples with HL filler (Fig. 4a) have the highest stiffness compared to FA and L mastics in all  $\omega_r$  and  
 274 f/b ratio domains. At 10°C the HL filler generates a stiffness of 49 MPa for the 1.25 f/b ratio, which  
 275 subsequently drops to 21.41-10<sup>-6</sup> MPa, for the f/b ratio equal to 0.50 at a frequency of 1.59Hz.

276 On the contrary, the samples with FA generate a maximum of 46 MPa for f/b equal to 1.25, and  
 277 consecutively decreases by 31 MPa, for the lowest dosage (f/b equal to 0.50), generating a greater variation  
 278 in the values of  $|G^*|$ , and causing a 16.54% difference compared to the HL filler.

279 This variation of the complex modulus  $|G^*|$  product of the increase of the f/b ratio is produced due  
 280 to the great stiffness capacity obtained by the HL filler, generating an inflexion point for lower  $\omega_r$ , due to  
 281 the greater amount of fine particles that this filler has, compared to the FA filler (Table 2).

282 However, when comparing the rheological behaviour of FA with L filler, an increase in the  
 283 difference in the values of the full modulus ( $|G^*|$ ) at a temperature of 10°C is obtained. The fly ash mastics  
 284 generate 66.69% higher stiffness compared to the L mastic. As the temperature increases (70°C), the values  
 285 of  $|G^*|$  increase without a large variation between the fillers, generating a parallel growth to that produced  
 286 by the B50/70 type bitumen (Figures 4b and 4c).

287 On the other hand, when fitting the curves by means of the sigmoidal function and determining  
 288 the  $I_{mastic}$  index (see Table 3), it is obtained that mastics with HL have a higher stiffness  $|G^*|$  per mass-  
 289 volume amount of the samples. The mastics with FA define a band of use with a larger area than the other  
 290 fillers with a growth of 91.52%, being more susceptible to variations in temperature and loading  
 291 frequencies. The mastics with filler L generate a difference in the values of the complex modulus  $|G^*|$  of  
 292 36.92%, on the variation of the dosage f/b. Finally, the mastics with filler HL generate a band of use with  
 293 a growth of 40.59% over the dosage of F/B 0.50. This slight difference of HL is due only to the rheological  
 294 capacity it acquires at elevated temperatures, being the only type of filler that reaches a stiffness of 108 Pa  
 295 for  $r$  of the order of 10-10 rad/s.

296 Referring to the output data of Eq (1), a growth of 10 Pa is obtained as the arithmetic mean between  
 297 the upper and lower asymptotes of all samples. The inflexion point is shifted to the right for the  $r$  values by

298  
299  
300

adding FA filler, HL and L. The slope of the sigmoidal curve is directly proportional to the amount of filler placed in the mixture, generating higher values of  $|G^*|$  at lower  $\omega_r$ .

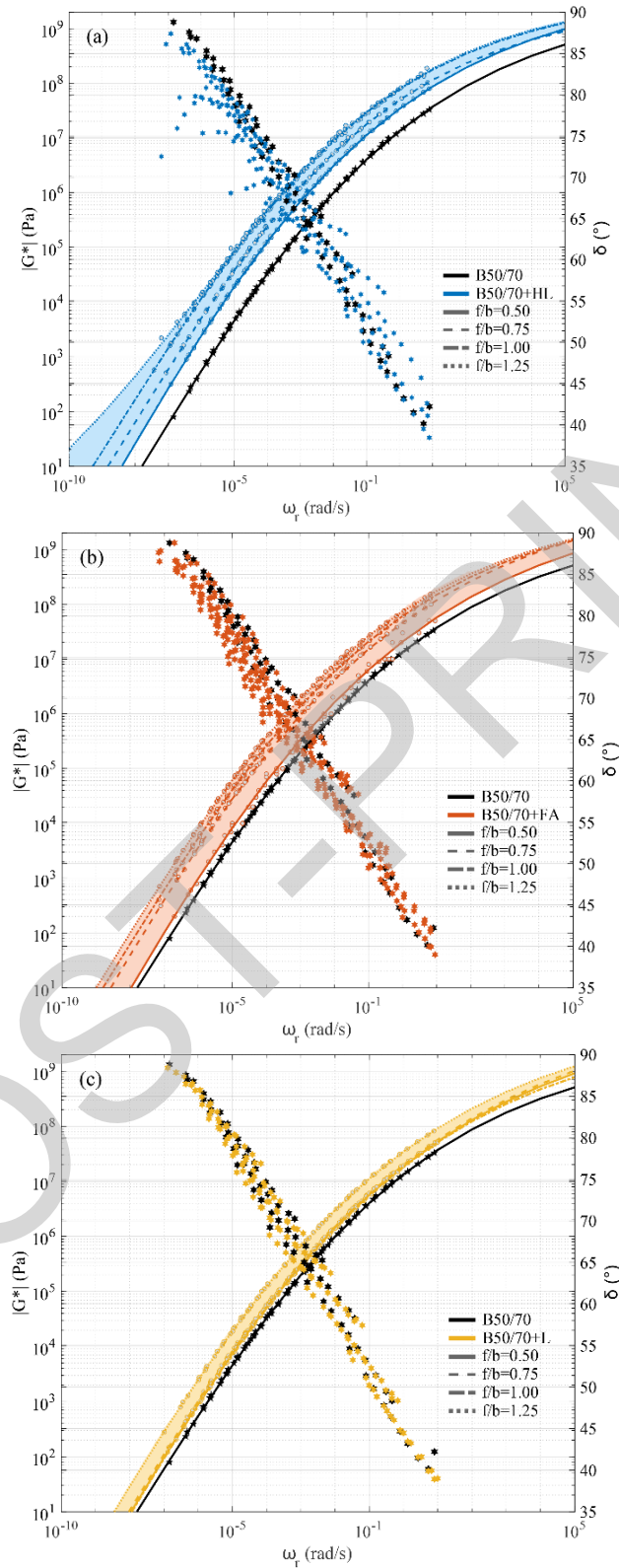


Figure 4. Master curve of the  $|G^*|$  and  $\delta$  for asphalt mastics. a) HL; b) FA; c) L

301

Table 3. Parameters of a master curve for asphalt bitumen and mastics

Type	$I_{mastic}$	$f/b$	$\alpha$	$\lambda$	$\varphi$	$\gamma$	$a_1 \cdot 10^{-4}$	$a_2$	$a_3$	$R^2$
B50/70	-	-	-7.32	16.86	-1.79	0.23	7.18	-0.15	0.0076	0.99

B50/70 + HL	40.59%	0.50	-8.89	18.70	-1.97	0.22	7.04	-0.15	0.0075	0.99
		0.75	-6.02	15.54	-2.01	0.25	7.52	-0.15	0.0075	0.99
		1.00	-5.80	15.47	-2.04	0.25	8.64	-0.16	0.0075	0.99
		1.25	-1.49	11.07	-1.72	0.28	7.54	-0.15	0.0076	0.99
B50/70 + FA	91.52%	0.50	-10.57	20.50	-1.92	0.21	6.70	-2.14	0.0075	0.99
		0.75	-10.40	20.50	-2.00	0.21	7.73	-0.15	0.0076	0.99
		1.00	-7.68	17.58	-1.99	0.23	7.92	-0.15	0.0075	0.99
		1.25	-7.69	17.58	-2.04	0.23	7.78	-0.15	0.0075	0.99
B50/70 + L	36.92%	0.50	-11.72	21.85	-1.89	0.19	7.08	-0.14	0.0076	0.99
		0.75	-11.70	21.91	-1.87	0.19	6.89	-0.14	0.0076	0.99
		1.00	-10.41	20.32	-1.90	0.21	6.06	-0.13	0.0076	0.99
		1.25	-9.54	19.60	-1.91	0.21	7.13	-0.14	0.0076	0.99

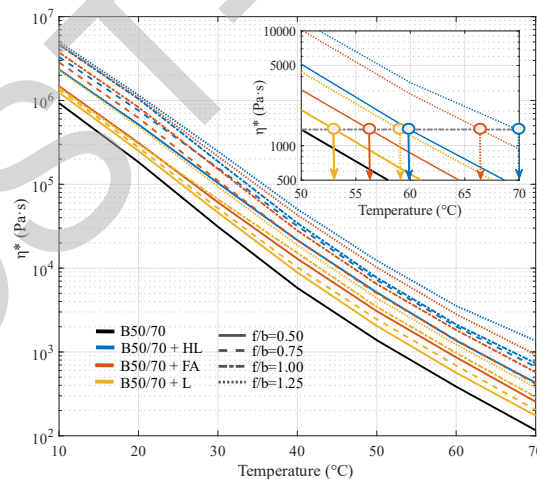
302  
303  
304  
305  
306  
307  
308  
309  
310  
311  
312  
313  
314  
315  
316  
317  
318  
319  
320

Figure 5 shows the complex viscosity  $\eta^*$  of bitumen type B50/70 and asphalt mastics. The results show that the complex parameter decreases as the experimental temperature decreases, which is caused by the softening of the material and the reduction of its stiffness.

The addition of the different types of fillers shifts the bitumen standard curve to the right, allowing higher values  $\eta^*$  for any reference temperature. In particular, mastics with L filler have the lowest changes compared to HL filler and FA. The data show that for a reference viscosity of the bitumen at a temperature of 50°C, the same value is obtained at 53.0°C, 54.5°C, 57.2°C and 59.2°C for f/b dosages equal to 0.50, 0.75, 1.00 and 1.25, respectively for the L filler.

The mastics with FA present (for the same reference) a shift to the right up to temperatures of 56.3°C, 60.0°C, 62.4°C and 66.9°C for the proposed f/b increment, generating growth of 62.90% for the possible values of  $\eta^*$  about the L filler.

Finally, the mastics with HL filler are the ones that present the greatest differences about the standard curve of the B50/70 type bitumen. The results determined that for the f/b concentration equal to 0.5, a temperature of 59.9°C is obtained about the  $\eta^*$  value at 50°C of the B50/70 type bitumen. The f/b concentrations equal to 0.75, 1.00 and 1.25 of HL filler reach temperatures of 60.0°C, 62.40°C and 70.0°C, respectively. This increase in temperature determines an increase of 70.97% compared to the values obtained with L filler for f/b ratios 0.5-1.25.



**Figure 5.** Results of the complex viscosity of the bitumen and asphalt mastics

321  
322  
323  
324  
325  
326  
327  
328  
329  
330  
331  
332

### 3.2. Experimental analysis of the MSCR test

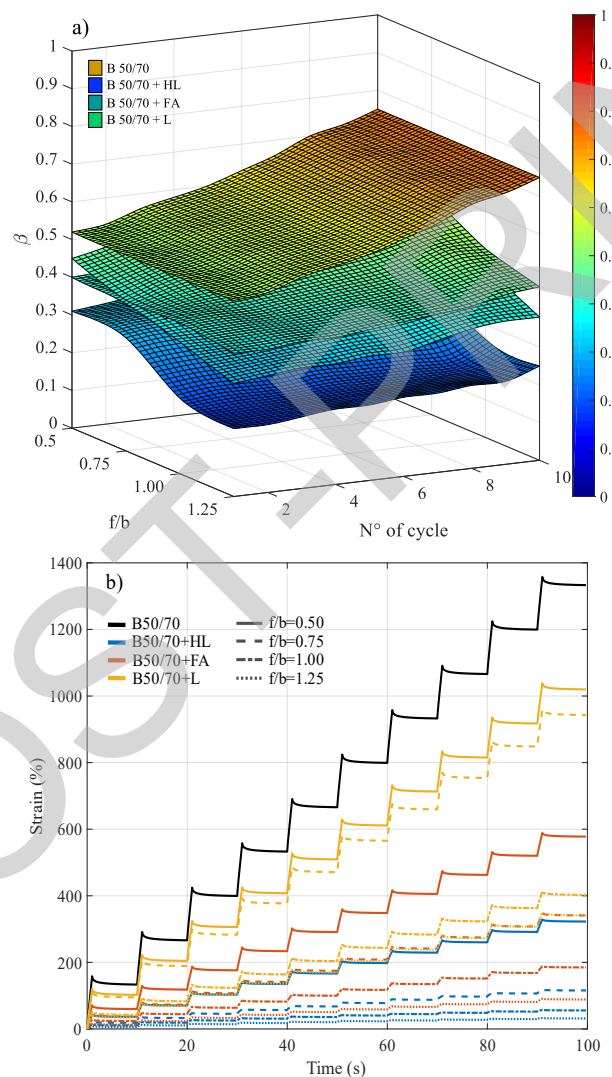
The deformations that appear when asphalt bitumen and mastic specimens subjected to creep and multiple recovery phenomena allow quantifying the contribution of the type of filler used and its relation with the bitumen mass. Therefore, it is possible to detail the rheological properties of the asphalt mastic by applying the model proposed, including the viscoelastic transition during the MSCR-test, which could cause permanent deformations in asphalt mixtures (see Appendix A).

Figure 6 shows the non-linear viscoelastic behaviour of the samples for a temperature of 50°C. The experimental data obtained show that bitumen type B50/70 presents an accumulated deformation of 1333.1%. However, when adding filler to this sample, it is determined that the L filler presents the highest deformations reaching a range of 341.34-1019.90% of accumulated deformation for the variation of f/b 0.50-1.25. Regarding the samples with FA filler a domain of 88.58-577.73% is reached presenting a

333 percentage difference of 43-74% of better mechanical performance, compared to the L filler for the same  
 334 variation. Finally, mastics with HL present the best performance recovering a large part of the deformation.  
 335 The values oscillate between 31.45-322.63% of accumulated deformation defining an improvement of 68-  
 336 91% in reference to the L filler for the limits  $f/b$  1.25-0.50, respectively.

337 To perform the mathematical adjustment of Eqs. (10) and (11) a computer code is developed. The  
 338 results (see Figure 6a) demonstrate the elastic influence of the type of filler used and its relation to the  $f/b$   
 339 dosage. First, the fit is established by Eq. (10) which indicates the characterization of the viscoelastic  
 340 deformations of the bitumen type B50/70. The fractional exponent  $\beta$  demonstrates the viscoelastic  
 341 transition of bitumen type B50/70 since when this value is 0, the material under study is considered a  
 342 completely elastic solid, while if it reaches the maximum value ( $\beta$  equal to 1), the material is considered a  
 343 Newtonian fluid.

344 In Figure 6a, it is observed that the bitumen type B50/70 at a temperature of 50°C reaches  $\beta$  0.52 for  
 345 the first cycle of the MSCR at 3.2 kPa. Subsequently, for the last test cycle, this value increases to a  
 346 maximum  $\beta_{\max}$  of 0.75, demonstrating the multiple stress softening capacity of bitumen type B50/70.  
 347



**Figure 6.** MSCR-test at 50°C. a) fractional exponent  $\beta$ ; b) experimental strain for 3.2 kPa

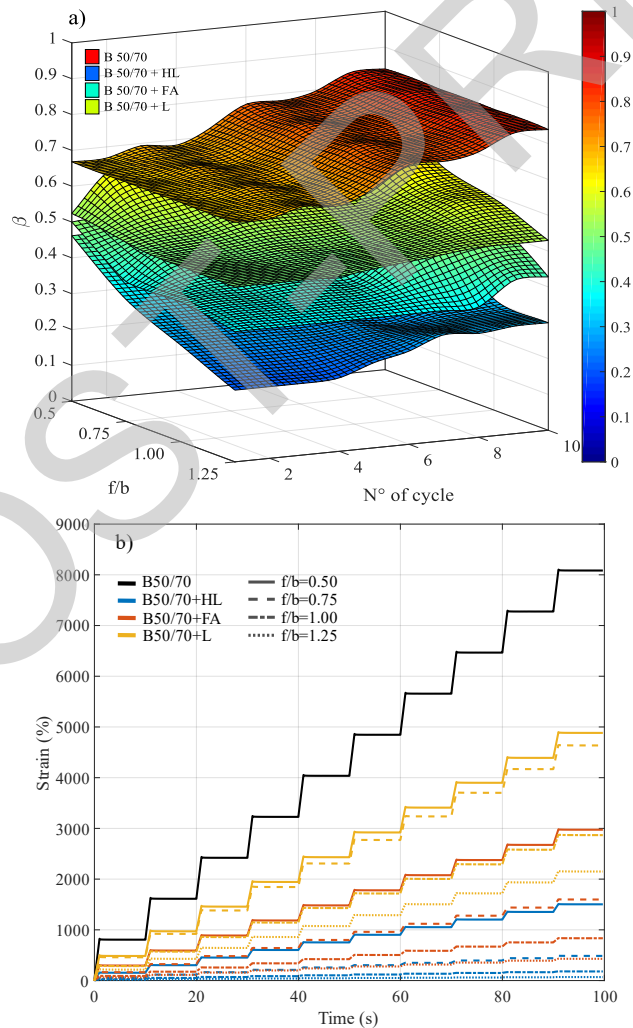
348 Subsequently, when adjusting the rheological model Eq. (11) for asphalt mastics, lower values  $\beta$   
 349 are reached due to the elastic capacity of the filler, which delays the state of deformation mentioned. The  
 350 samples with the lowest values  $\beta$  are those with HL filler, reaching a maximum value of 0.38, which drops  
 351 sharply as the filler concentration increases above the  $f/b$  dosage equal to 1.00 (see Figure 6a). L and FA  
 352 mastics have higher  $\beta$  values than those of HL, with a linear decrease of the parameter as the  $f/b$  ratio  
 353 increases. The maximum values  $\beta$  obtained for the filler surfaces with FA and L are 0.53 and 0.65 for the  
 354 maximum dosage, respectively.  
 355

356 Increasing the temperature up to a temperature of 60°C generates a greater difference in the results  
 357 between the bitumen and mastics compared to those obtained at 50°C. Figure 7b shows that bitumen type  
 358 B50/70 reaches 8084.6% deformation, generating a considerable increase in the viscoelastic transition with  
 359 respect to the 50°C temperature. For the viscoelastic simulation criteria, bitumen type B50/70 at 60°C (see  
 360 Fig. 7a), reaches a maximum value of  $\beta=0.84$  for the tenth cycle of the test, reaching a growth of 12%  
 361 compared to the previous temperature.

362 Mastics with L filler show the highest deformations among the types of filler studied. The range  
 363 of deformations is 2149-4882%, generating a softening product of multiple stress with value  $\beta$  of 0.48-  
 364 0.76, increasing by 16% the values for the variation of  $f/b$  equal to 0.5-1.25. In addition, mastics with FA  
 365 fillers present a range of 429-2974%, improving the behaviour compared to samples with L by 43-80% for  
 366  $f/b$  dosages equal to 1.25 to 0.50. The above shows that there are no differences in the behaviour shown by  
 367 the mastics at a temperature of 50°C between FA and L. Likewise, the mastics with FA increase the  
 368 viscoelastic transition  $\beta$  by 11% in reference to the 50°C temperature, demonstrating greater elasticity than  
 369 those made with L.

370 Finally, the samples with HL show the best behaviour under creep-recovery phenomena with a  
 371 domain of 68-1503% of accumulated deformation. Similarly to the samples with FA, the mastics with HL  
 372 maintain the percentage difference obtained at 50°C, defining an improvement of 69-91% in relation to the  
 373 behaviour of the samples with L.

374 The domain  $\beta$  for the samples with HL extends from 0.20 to 0.50, generating a behaviour with a  
 375 higher tendency to elasticity ( $\beta=0$ ) compared to FA and L. In contrast to the rheological simulation at  
 376 50°C, the samples with HL generated the greatest changes with 28% of the increase  $\beta$ .  
 377



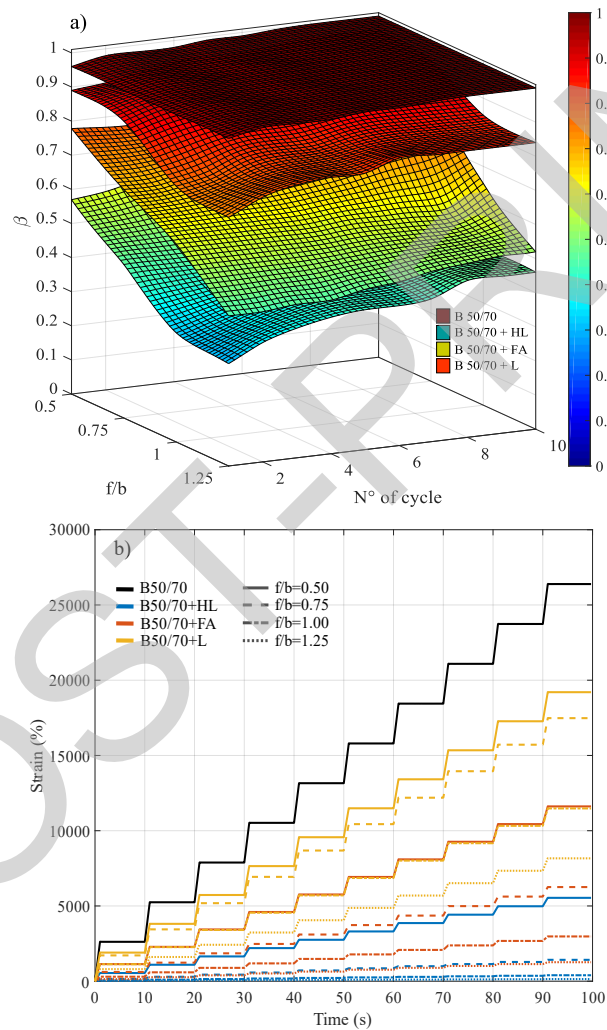
378 **Figure 7.** MSCR-test at 60°C. a) fractional exponent  $\beta$ ; b) experimental strain for 3.2 kPa

379 Figure 8 shows the rheological behaviour of the bitumen and asphalt mastics for a temperature of  
 380 70°C in the MSCR test. Bitumen type B50/70 is the sample with the highest deformation (26389%

381 accumulated; the rheological simulation (see Figure 8a) shows that the rheological values  $\beta$  reach a  
 382 minimum value of 0.96 for the first cycle, reaching the maximum value of  $\beta=1$ , demonstrating a Newtonian  
 383 fluid behaviour.

384 The samples with L filler acquire a deformation range from 8164% to 19205%, with an increase  
 385  $\beta$  of varying between 0.72-0.96 for the variation of  $f/b$  equal to 0.5-1.25. The mastics with FA present a  
 386 deformable range of 1261-6255%, which increases the range obtained at a temperature of 60°C, obtaining  
 387 an improvement in the performance of 40-84%, compared to the samples with L, for the range of  $f/b$  equal  
 388 to 1.25 to 0.50. The transition of the parameter  $\beta$  for the samples with FA ends in an interval 0.44-0.95,  
 389 which shows a maximum growth of 36% for the  $f/b$  ratio equal to 0.50.

390 The HL filler generates the best performance when mixed with bitumen type B50/70 compared to  
 391 the rest of the fillers. The results indicate a domain of 140-5539% of accumulated deformation, being 71%  
 392 more efficient than the L samples for  $f/b$  equal to 0.50, and reaching 98% for the dosage of  $f/b$  equal to  
 393 1.25. With respect to the normalization of the vector  $\beta$ , a final domain is obtained for HL mastics at 70°C  
 394 from 0.30 to 0.78, being the filler that generates the highest elasticity.  
 395



396 **Figure 8.** MSCR-test at 70°C. a) fractional exponent  $\beta$ ; b) experimental strain for 3.2 kPa

397 In addition to the degree of viscoelasticity obtained with the fractional derivative  $\beta$ , the proposed  
 398 model for mastic asphalt (Figure 3b) allows detailing the elastic capacity  $\xi_2$  of the different fillers, due to  
 399 the infinitesimal representation of the mineral aggregate enveloped by the asphalt bitumen. The results  
 400 (Table 4) determine that for the 10 cycles of the MSCR at 3.2 kPa, the elastic property  $\xi_2$  increases as a  
 401 higher concentration of filler is added to the sample.

402 In particular, when comparing the types of fillers, it is observed that a higher Young's modulus is  
 403 quantified for the samples with HL in the four dosages analyzed. This elastic difference is greater for the  
 404 filler/bitumen ratios with higher filler content, demonstrating that the mathematical adjustment allows

405 detailing the elasticity as a function of the nature of the filler and its relation to the mass of the asphalt  
 406 bitumen.

407 In this sense, the samples with HL filler present a greater elastic difference of  $4.67 \cdot 10^{-3}$  kPa for  
 408 the highest f/b concentration at 50°C. Subsequently, this difference decreases with decreasing filler content,  
 409 reaching  $5.9 \cdot 10^{-4}$  kPa for f/b ratio equal to 1.00 and  $9.00 \cdot 10^{-6}$  kPa for f/b ratio equal to 0.75. Otherwise,  
 410 the model is not able to predict a difference for the f/b concentration equal to 0.50 between the HL and FA  
 411 fillers, characterizing the same Young's modulus for 50°C, which is due to the similarity of the mechanical  
 412 behaviour for low concentrations.

413 When analyzing the L filler, it is observed that the model shows even lower values than those  
 414 obtained with HL and FA. The greatest difference is observed for the dosage f/b equal to 1.25, where a  
 415 percentage difference of 99.99% is obtained in the values of  $\xi_2$  when compared with the HL filler. Likewise,  
 416 the sample with FA presents a 99.28% higher elasticity in contrast to the L filler.

417 Based on the lower dosage (f/b equal to 0.50), the model characterizes Young's modulus for the L  
 418 filler with values different from those shown for the HL and FA fillers, which is directly related to the  
 419 fineness of the filler used. In summary, the mathematical model is able to differentiate an elasticity  $\xi_2$  for  
 420 the type of filler at low concentrations (f/b equal to 0.50) only when there is a difference in the particle  
 421 sizes as presented in this study (see Table 2).

422 When increasing the test temperature to 60 and 70°C, the output  $\xi_2$  values of the different mastics  
 423 do not show large differences. Therefore, an ANOVA statistical analysis of the 10-cycle MSCR setting at  
 424 3.2 kPa is performed for all dosages and temperatures. Table 5 shows the values of the variance of parameter  
 425 2. It is obtained that the filler with HL and L presents a P-value of 99%, accepting the hypothesis that the  
 426 elasticity  $\xi_2$  of the type of filler is not affected when the temperature increases from 50°C to 70°C. In the  
 427 case of FA, the elasticity obtained generates a greater dispersion of the data, obtaining a probability of  
 428 success of 95.64%, which can be attributed to a possible chemical interaction between the filler/bitumen  
 429 interface.

430

**Table 4.** Elasticity parameter  $\xi_2$  (kPa) for asphalt mastics

Type	f/b	Temperature		
		50°C	60°C	70°C
B50/70 + HL	1.25	$4.70 \cdot 10^{-3}$	$4.65 \cdot 10^{-3}$	$4.70 \cdot 10^{-3}$
	1.00	$6.00 \cdot 10^{-4}$	$5.80 \cdot 10^{-4}$	$6.00 \cdot 10^{-4}$
	0.75	$1.00 \cdot 10^{-5}$	$1.00 \cdot 10^{-5}$	$1.00 \cdot 10^{-5}$
	0.50	$2.00 \cdot 10^{-14}$	$2.25 \cdot 10^{-14}$	$2.00 \cdot 10^{-14}$
B50/70 + FA	1.25	$3.00 \cdot 10^{-5}$	$3.19 \cdot 10^{-5}$	$3.00 \cdot 10^{-5}$
	1.00	$1.00 \cdot 10^{-5}$	$1.08 \cdot 10^{-5}$	$1.00 \cdot 10^{-5}$
	0.75	$1.01 \cdot 10^{-6}$	$1.10 \cdot 10^{-6}$	$1.00 \cdot 10^{-6}$
	0.50	$2.00 \cdot 10^{-14}$	$3.16 \cdot 10^{-14}$	$2.00 \cdot 10^{-14}$
B50/70 + L	1.25	$2.16 \cdot 10^{-7}$	$2.15 \cdot 10^{-7}$	$2.16 \cdot 10^{-7}$
	1.00	$5.00 \cdot 10^{-12}$	$1.46 \cdot 10^{-12}$	$1.40 \cdot 10^{-12}$
	0.75	$2.17 \cdot 10^{-12}$	$2.16 \cdot 10^{-12}$	$2.17 \cdot 10^{-12}$
	0.50	$4.42 \cdot 10^{-14}$	$4.42 \cdot 10^{-14}$	$4.40 \cdot 10^{-14}$

431

**Table 5.** Anova for  $\xi_2$

Source of variability	Sum of squares	Degrees of freedom	Mean squares	F-statistic	P-value
B50/70 + HL	0	2	$3.66307 \cdot 10^{-9}$	0	0.9993
Error	0.00059	117	$5.08114 \cdot 10^{-6}$	-	-
Total	0.00059	119	-	-	-
B50/70 + FA	$1.39096 \cdot 10^{-11}$	2	$6.95479 \cdot 10^{-12}$	0.04	0.9564
Error	$1.82610 \cdot 10^{-8}$	117	$1.56077 \cdot 10^{-10}$	-	-
Total	$1.82749 \cdot 10^{-8}$	119	-	-	-
B50/70 + L	$3.9103 \cdot 10^{-9}$	2	$1.95515 \cdot 10^{-19}$	$8.81016 \cdot 10^{-6}$	0.9999
Error	$2.59646 \cdot 10^{-12}$	117	$1.95551 \cdot 10^{-14}$	-	-
Total	$2.59646 \cdot 10^{-12}$	119	-	-	-

432

433 Figure 9a shows the relationship between  $J_{nr,3.2}$  and  $R_{3.2}$  for bitumen type B50/70 and asphalt  
 434 mastics. The results indicate that with increasing temperature, higher  $J_{nr}$  values are generated with lower  
 435 recovery, due to the transformation from viscoelastic to the viscous state of the samples.

436 In particular, for a temperature of 50°C, the mastics with L have the same  $R_{3.2}$  range as the bitumen  
 437 type B50/70 for f/b concentrations equal to 0.50-0.75. However, a mismatch is generated, obtaining lower

438 creep deformations  $J_{nr,3,2}$ , so it is necessary to calculate the  $J_{nr}/R$  ratio to establish a performance index and  
 439 quantify the elasticity of the fillers. Now, if the amount of  $J_{nr}$  due to  $R$  recovery is analyzed, it is observed  
 440 that mastics with L filler present an improvement of 21-80% of  $J_{nr}/R$  in comparison to bitumen type B50/70  
 441 for the variation  $f/b$  equal to 0.50-1.25 $f$ . In contrast, HL and FA fillers achieve an improvement between  
 442 78-99% and 59-95% respectively, determining better  $J_{nr}/R$  ratios for the same  $f/b$  variation. Subsequently,  
 443 as the temperature increases, greater differences are generated between mastics and bitumen, showing an  
 444 increase in the  $J_{nr}/R$  index of 91-99.93% for HL, 76-98% for FA and 60-89% for L filler in reference to  
 445 bitumen type B50/70.

446 Figure 9b shows a comparison between the results obtained in the LVE range with the damage  
 447 obtained in the MSCR cumulative damage test for asphalt mastics. In relating these phenomena, it is  
 448 necessary to specify that the parameter  $|G^*|/\sin(\delta)$  is able to normalize an index for rutting failures for  
 449 bitumens, but not for mastics ( $|G^*|/\sin(\delta) > 1.00 \text{ kPa}$ ). In this case, when comparing samples with fillers, it  
 450 is observed that  $|G^*|/\sin(\delta)$  has a significant influence due to temperature. In particular, the  $|G^*|/\sin(\delta)$  and  
 451 the reciprocal of  $J_{nr,3,2}$  have the same units (kPa) and when correlating their results for angular velocity 10  
 452 rad/s and temperatures of 50, 60 and 70°C (see Fig. 6b), a good *Pearson* correlation of  $\rho=0.82$  is obtained,  
 453 although not strong for  $p\text{-value} < 0.05$ . This trend is generated due to the fact that independent of the test  
 454 procedure, the samples decrease their stiffness as the test temperature increases, showing a higher value  $\beta$   
 455 or softening. In the particular case for a test temperature, the samples increase their stiffness as the dosage  
 456  $f/b$  increases, but they soften as a result of the repetitive loads measured by  $\beta$ .  
 457

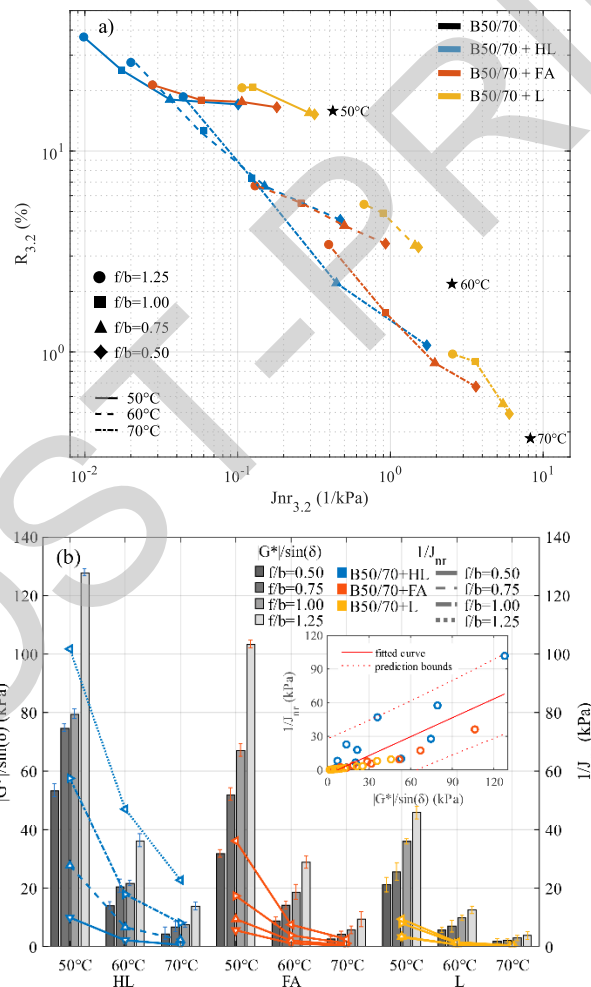


Figure 9. MSCR values of asphalt mastics with different  $f/b$  ratio. a)  $J_{nr,3,2}$  v/s  $R$  values; b)  $|G^*|/\sin(\delta)$  and  $J_{nr,3,2}$  values

458  
 459  
 460  
 461  
 462

#### 4. CONCLUSIONS

In the present investigation, the viscoelastic behaviour of asphalt mastics with three different types of fillers (HL, FA and L) at high and low temperatures analyzed using a DSR. The results obtained in this research demonstrate that the use of the rheological model proposed allows detailing the elastic capacity of

463 the fillers and viscoelastic capacity of the bitumen for the multiple stress of the MSCR. The main  
 464 conclusions of the study presented below:  
 465

- 466 • The viscoelasticity model proposed in this paper represents a detailed way to mechanically  
 467 characterize asphalt mastics. Unlike the classical viscoelastic models, the new proposed  
 468 model allows detailing the elastic  $\xi_2$  influence of the fillers, the viscoelasticity of the asphalt  
 469 bitumen and its relationship with the  $f/b$  dosage used for an  $f/b$  range of 0.5 to 1.25.
- 470 • The use of fractional derivatives in the proposed model for the bitumen and asphalt mastics  
 471 results in new terms in the MSCR test recovery modulus equation. The parameter  $\beta$  explains  
 472 more precisely the total energy release caused by the bitumen and mastic asphalt, quantifying  
 473 the viscoelastic transition of the filler/bitumen system for the 10 cycles of 3.2 kPa, generating  
 474 a study of the impact of the filler type and its relationship with the filler/bitumen dosage.
- 475 • The rheological analyses of the B50/70 type bitumen and the asphalt mastics have made it  
 476 possible to quantify the effect of the fillers on the resulting mastics. The results obtained show  
 477 that the samples with HL generate higher stiffness values  $|G^*|$  and lower accumulated  
 478 deformations  $R$ , compared to the FA filler, due to the greater fineness of its particles. In  
 479 addition, a large development of the elastic capacity  $\xi_2$  or Young's modulus is demonstrated,  
 480 being directly proportional to the filler/bitumen ratio.
- 481 • In the future, further work is planned to obtain a complete design of asphalt mixtures,  
 482 comparing the methodology of the present study with the development of bitumens, mastics  
 483 and asphalt mixtures for fatigue and permanent deformation phenomena. This will help  
 484 determine the influence of bitumen modifying materials on the behaviour of asphalt mastics.  
 485

#### 486 ACKNOWLEDGEMENTS

487 The authors gratefully acknowledge the institutional support provided by the Vice-Rector for Research,  
 488 Development and Artistic Creation of the University Austral of Chile (VIDCA UACH), to the Santander  
 489 Bank Iberoamerican Scholarship Program, and the pavements lab of the Faculty of Engineering Sciences.  
 490 Besides, to the GITECO and GCS research groups from the University of Cantabria (Spain) for their  
 491 support.  
 492

#### 493 FUNDING SOURCES

494 This work was supported by the National Research and Development Agency (ANID) of Chile  
 495 [FONDECYT Regular N°1211160] and [FONDECYT Regular N°1201029].  
 496

#### 497 Appendix A

498 In this appendix some examples of the problem discussed in the main text on the permanent  
 499 deformations of bitumen B50/70 and the asphalt mastics studied are illustrate.

500 First, Eq. (10) is used to adjust the recovery phenomenon in the bitumen at 50°C in the 10 cycles  
 501 independently (see Fig. 10). This procedure is achieved by means of computer codes using MATLAB®,  
 502 defining the domain of elastic-viscous rheological properties of B50/70,  $\xi_1$  and  $\beta$  respectively. The  
 503 fractional derivative  $\beta$  is obtained as an indicator of the recoverable non-linear viscoelasticity,  
 504 demonstrating the change between the elastic and viscous state (see Figures 6, 7 and 8).  
 505

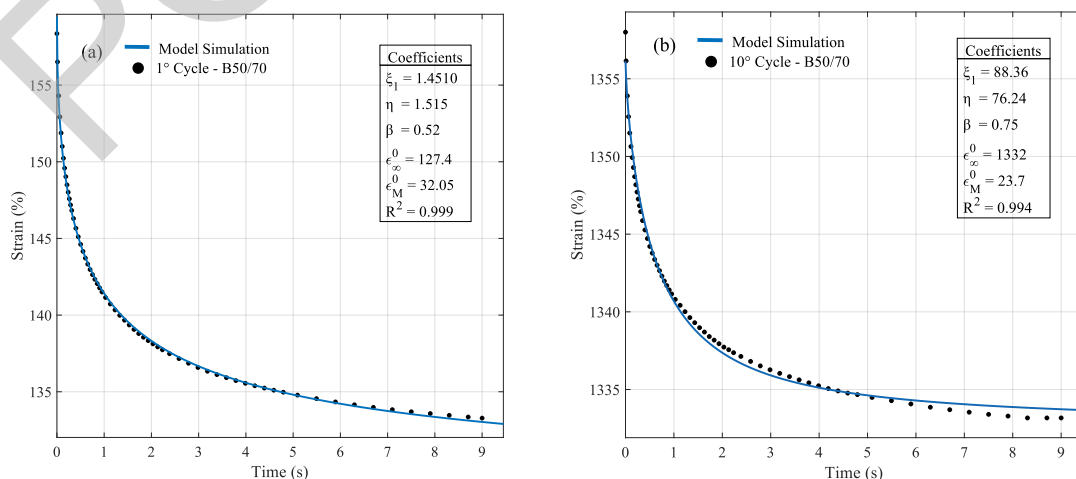


Figure 10. Rheological simulation of bitumen B50/70 for 3.2 kPa and 50°C. a) 1°cycle; b)10°cycle

506  
507  
508  
509  
510  
511

Once the B50/70 parameters have been obtained, the adjustment is defined by means of Eq. (11) (see Fig. 11) for the MSCR in asphalt mastics. For this adjustment, the elastic capacity of each filler ( $\xi_2$ ) and its relation with the bitumen mass ( $f/b$ ) are defined. The same procedure was used for all the combinations and temperatures studied.

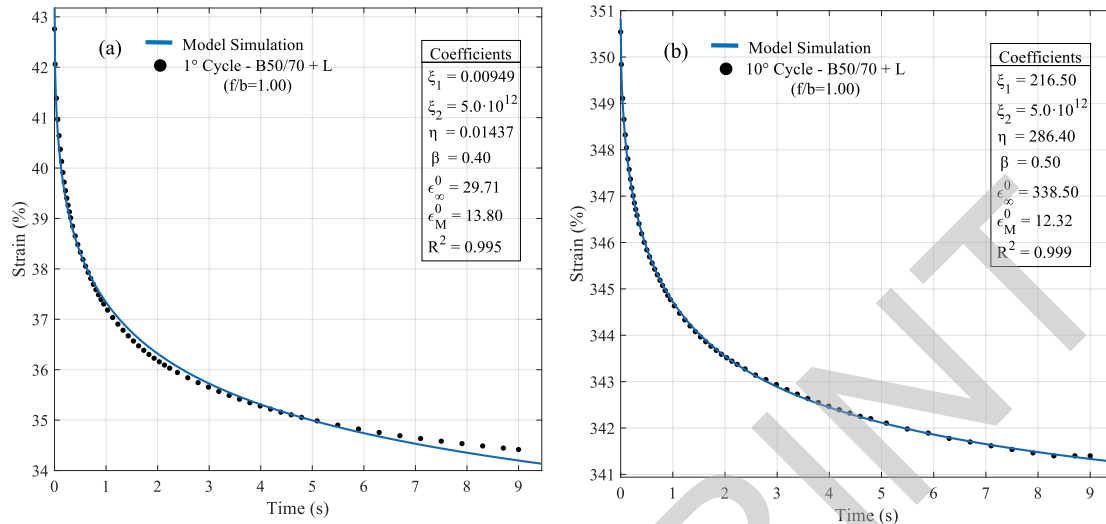


Figure 11. Rheological simulation of limestone asphalt mastic for 3.2 kPa and 50°C. a) 1°cycle; b)10°cycle

512  
513  
514  
515  
516  
517  
518  
519  
520  
521  
522  
523  
524  
525  
526  
527  
528  
529  
530  
531  
532  
533  
534  
535  
536  
537  
538  
539  
540  
541  
542  
543  
544  
545

## REFERENCES

- [1] M. Lagos-Varas, D. Movilla-Quesada, J.P. Arenas, A.C. Raposeiras, D. Castro-Fresno, M.A. Calzada-Pérez, A. Vega-Zamanillo, J. Maturana, Study of the mechanical behavior of asphalt mixtures using fractional rheology to model their viscoelasticity, *Construction and Building Materials*. 200 (2019). doi:10.1016/j.conbuildmat.2018.12.073.
- [2] A. Arabzadeh, H. Ceylan, S. Kim, A. Sassani, K. Gopalakrishnan, M. Mina, Electrically-conductive asphalt mastic: Temperature dependence and heating efficiency, *Materials & Design*. 157 (2018) 303–313. doi:10.1016/j.matdes.2018.07.059.
- [3] M. Zaumanis, L.D. Poulidakos, M.N. Partl, Performance-based design of asphalt mixtures and review of key parameters, *Materials & Design*. 141 (2018) 185–201. doi:10.1016/j.matdes.2017.12.035.
- [4] F. Russo, R. Veropalumbo, L. Pontoni, C. Oreto, S.A. Biancardo, N. Viscione, F. Pirozzi, M. Race, Sustainable asphalt mastics made up recycling waste as filler, *Journal of Environmental Management*. 301 (2022). doi:10.1016/j.jenvman.2021.113826.
- [5] X. Zhu, Y. Yuan, L. Li, Y. Du, F. Li, Identification of interfacial transition zone in asphalt concrete based on nano-scale metrology techniques, *Materials & Design*. 129 (2017) 91–102. doi:10.1016/j.matdes.2017.05.015.
- [6] M. Guo, A. Motamed, Y. Tan, A. Bhasin, Investigating the interaction between asphalt binder and fresh and simulated RAP aggregate, *Materials & Design*. 105 (2016) 25–33. doi:10.1016/j.matdes.2016.04.102.
- [7] D. Movilla-Quesada, Á. Vega-Zamanillo, M.Á. Calzada-Pérez, D. Castro-Fresno, Evaluation of water effect on bituminous mastics with different contribution fillers and binders, *Construction and Building Materials*. 29 (2012) 339–347. doi:10.1016/j.conbuildmat.2011.08.093.
- [8] J. Wang, M. Guo, Y. Tan, International Journal of Transportation Study on application of cement substituting mineral fillers in asphalt mixture, *International Journal of Transportation Science and Technology*. 7 (2018) 189–198. doi:10.1016/j.ijtst.2018.06.002.
- [9] D. Movilla-Quesada, O. Muñoz, A.C. Raposeiras, D. Castro-Fresno, Thermal susceptibility analysis of the reuse of fly ash from cellulose industry as contribution filler in bituminous mixtures, *Construction and Building Materials*. 160 (2018) 268–277. doi:10.1016/j.conbuildmat.2017.11.046.
- [10] A.K. Das, D. Singh, Investigation of rutting, fracture and thermal cracking behavior of asphalt mastic containing basalt and hydrated lime fillers, *Construction and Building Materials*. 141 (2017) 442–452. doi:10.1016/j.conbuildmat.2017.03.032.

- 546 [11] C. Li, Z. Chen, S. Wu, B. Li, J. Xie, Y. Xiao, Effects of steel slag fillers on the rheological  
547 properties of asphalt mastic, 145 (2017) 383–391. doi:10.1016/j.conbuildmat.2017.04.034.
- 548 [12] Y. Li, S. Liu, Z. Xue, W. Cao, Experimental research on combined effects of flame retardant and  
549 warm mixture asphalt additive on asphalt binders and bituminous mixtures, *Construction and*  
550 *Building Materials*. 54 (2014) 533–540. doi:10.1016/j.conbuildmat.2013.12.058.
- 551 [13] C. Viet, P. Hervé, D. Benedetto, C. Sauzéat, D. Lesueur, S. Pouget, Influence of hydrated lime  
552 on linear viscoelastic properties of bituminous mastics, *Mech Time-Depend Mater.* (2019).  
553 doi:10.1007/s11043-018-09404-x.
- 554 [14] K. Wu, K. Zhu, C. Kang, B. Wu, Z. Huang, An experimental investigation of flame retardant  
555 mechanism of hydrated lime in asphalt mastics, *Materials & Design*. 103 (2016) 223–229.  
556 doi:10.1016/j.matdes.2016.04.057.
- 557 [15] D. Lesueur, D. N. Little, Effect of Hydrated Lime on Rheology, Fracture, and Aging of Bitumen,  
558 *Transportation Research Record*. 1661(1999) 93–105. doi:10.3141/1661-14
- 559 [16] É. Lachance-Tremblay, D. Perraton, M. Vaillancourt, H. Di Benedetto, Effect of hydrated lime  
560 on linear viscoelastic properties of asphalt mixtures with glass aggregates subjected to freeze-  
561 thaw cycles, *Construction and Building Materials*. 184 (2018) 58–67.  
562 doi:10.1016/j.conbuildmat.2018.06.130.
- 563 [17] F. Maghool, A. Arulrajah, Y. Du, S. Horpibulsuk, A. Chinkulkijniwat, Environmental impacts of  
564 utilizing waste steel slag aggregates as recycled road construction materials *Environmental*  
565 *impacts of utilizing waste steel slag aggregates as recycled road construction materials*, *Clean*  
566 *Technologies and Environmental Policy*. (2017). doi:10.1007/s10098-016-1289-6.
- 567 [18] A. Wozuk, L. Bandura, W. Franus, Fly ash as low cost and environmentally friendly filler and  
568 its effect on the properties of mix asphalt, *Journal of Cleaner Production*. 235 (2019) 493–502.  
569 doi:10.1016/j.jclepro.2019.06.353.
- 570 [19] R. Mistry, T. Kumar, Effect of using fly ash as alternative filler in hot mix asphalt, *Perspectives*  
571 *in Science*. 8 (2016) 307–309. doi:10.1016/j.pisc.2016.04.061.
- 572 [20] F. Li, Y. Yang, L. Wang, Evaluation of physicochemical interaction between asphalt binder and  
573 mineral filler through interfacial adsorbed film thickness, *Construction and Building Materials*.  
574 252 (2020) 119135. doi:10.1016/j.conbuildmat.2020.119135.
- 575 [21] T. Ma, D. Zhang, Y. Zhang, Y. Zhao, X. Huang, Effect of air voids on the high-temperature  
576 creep behavior of asphalt mixture based on three-dimensional discrete element modeling,  
577 *Materials & Design*. 89 (2016) 304–313. doi:10.1016/j.matdes.2015.10.005.
- 578 [22] X. Ding, T. Ma, L. Gu, Y. Zhang, Investigation of surface micro-crack growth behavior of  
579 asphalt mortar based on the designed innovative mesoscopic test, *Materials & Design*. 185  
580 (2020) 108238. doi:10.1016/j.matdes.2019.108238.
- 581 [23] M. Lagos-Varas, D. Movilla-Quesada, A.C. Raposeiras, J.P. Arenas, M.A. Calzada-Pérez, A.  
582 Vega-Zamanillo, P. Lastra-González, Influence of limestone filler on the rheological properties  
583 of bituminous mastics through susceptibility master curves, *Construction and Building Materials*.  
584 231 (2020). doi:10.1016/j.conbuildmat.2019.117126.
- 585 [24] F. Safaei, C. Castorena, Material nonlinearity in asphalt binder fatigue testing and analysis,  
586 *Materials & Design*. 133 (2017) 376–389. doi:10.1016/j.matdes.2017.08.010.
- 587 [25] D. Movilla-Quesada, O. Muñoz, A.C. Raposeiras, D. Castro-Fresno, Thermal susceptibility  
588 analysis of the reuse of fly ash from cellulose industry as contribution filler in bituminous  
589 mixtures, *Construction and Building Materials*. 160 (2018) 268–277.  
590 doi:10.1016/j.conbuildmat.2017.11.046.
- 591 [26] R.J. Jackson, A. Wojcik, M. Miodownik, 3D printing of asphalt and its effect on mechanical  
592 properties, *Materials & Design*. 160 (2018) 468–474. doi:10.1016/j.matdes.2018.09.030.
- 593 [27] M. Han, J. Li, Y. Muhammad, Y. Yin, J. Yang, S. Yang, S. Duan, Studies on the secondary  
594 modification of SBS modified asphalt by the application of octadecyl amine grafted graphene  
595 nanoplatelets as modifier, *Diamond and Related Materials*. 89 (2018) 140–150.  
596 doi:10.1016/j.diamond.2018.08.011.
- 597 [28] A. Jamshidi, M.O. Hamzah, K. Kurumisawa, T. Nawa, B. Samali, Evaluation of sustainable  
598 technologies that upgrade the binder performance grade in asphalt pavement construction,  
599 *Materials & Design*. 95 (2016) 9–20. doi:10.1016/j.matdes.2016.01.065.
- 600 [29] Y. Sun, W. Wang, J. Chen, Investigating impacts of warm-mix asphalt technologies and high  
601 reclaimed asphalt pavement binder content on rutting and fatigue performance of asphalt binder  
602 through MSCR and LAS tests, *Journal of Cleaner Production*. 219 (2019) 879–893.  
603 doi:10.1016/j.jclepro.2019.02.131.

- 604 [30] C. Wang, Y. Wang, Physico-chemo-rheological characterization of neat and polymer-modified  
605 asphalt binders, *Construction and Building Materials*. 199 (2019) 471–482.  
606 doi:10.1016/j.conbuildmat.2018.12.064.
- 607 [31] E. Dubois, D.Y. Mehta, A. Nolan, Correlation between multiple stress creep recovery (MSCR)  
608 results and polymer modification of binder, *Construction and Building Materials*. 65 (2014) 184–  
609 190. doi:10.1016/j.conbuildmat.2014.04.111.
- 610 [32] K. Hu, C. Yu, Q. Yang, Y. Chen, G. Chen, R. Ma, Multi-scale enhancement mechanisms of  
611 graphene oxide on styrene-butadiene-styrene modified asphalt: An exploration from molecular  
612 dynamics simulations, *Materials & Design*. 208 (2021) 109901.  
613 doi:10.1016/j.matdes.2021.109901.
- 614 [33] J. Zhang, L.F. Walubita, A.N.M. Faruk, P. Karki, G.S. Simate, Use of the MSCR test to  
615 characterize the asphalt binder properties relative to HMA rutting performance – A laboratory  
616 study, *Construction and Building Materials*. 94 (2015) 218–227.  
617 doi:10.1016/j.conbuildmat.2015.06.044.
- 618 [34] P. Li, X. Jiang, K. Guo, Y. Xue, H. Dong, Analysis of viscoelastic response and creep  
619 deformation mechanism of asphalt mixture, *Construction and Building Materials*. 171 (2018)  
620 22–32. doi:10.1016/j.conbuildmat.2018.03.104.
- 621 [35] X. Zhu, Y. Sun, C. Du, W. Wang, J. Liu, J. Chen, Rutting and fatigue performance evaluation of  
622 warm mix asphalt mastic containing high percentage of artificial RAP binder, *Construction and  
623 Building Materials*. 240 (2020) 117860. doi:10.1016/j.conbuildmat.2019.117860.
- 624 [36] M. Lagos-varas, A.C. Raposeiras, D. Movilla-quesada, J.P. Arenas, D. Castro-fresno, O. Muñoz-  
625 Cáceres, V.C. Andres-Valeri, Study of the permanent deformation of binders and asphalt  
626 mixtures using rheological models of fractional viscoelasticity, *Construction and Building  
627 Materials*. 260 (2020) 120438. doi:10.1016/j.conbuildmat.2020.120438.
- 628 [37] J. Zhang, C. Sun, P. Li, M. Liang, H. Jiang, Z. Yao, Experimental study on rheological  
629 properties and moisture susceptibility of asphalt mastic containing red mud waste as a filler  
630 substitute, *Construction and Building Materials*. 211 (2019) 159–166.  
631 doi:10.1016/j.conbuildmat.2019.03.252.
- 632 [38] E.-C. Tsardaka, M. Stefanidou, Study of the action of nano-alumina particles in hydrated lime  
633 pastes, *Journal of Building Engineering*. 46 (2022) 103808. doi:10.1016/j.job.2021.103808.
- 634 [39] H. Naveed, Z. ur Rehman, A. Hassan Khan, S. Qamar, M.N. Akhtar, Effect of mineral fillers on  
635 the performance, rheological and dynamic viscosity measurements of asphalt mastic,  
636 *Construction and Building Materials*. 222 (2019) 390–399.  
637 doi:10.1016/j.conbuildmat.2019.06.170.
- 638 [40] Q. Li, C. Zhu, H. Zhang, S. Zhang, Evaluation on long-term performance of emulsified asphalt  
639 cold recycled mixture incorporating fly ash by mechanistic and microscopic characterization,  
640 *Construction and Building Materials*. 319 (2022) 126120.  
641 doi:10.1016/j.conbuildmat.2021.126120.
- 642 [41] S. Xu, X. Liu, A. Tabaković, P. Lin, Y. Zhang, S. Nahar, B.J. Lommerts, E. Schlangen, The role  
643 of rejuvenators in embedded damage healing for asphalt pavement, *Materials & Design*. 202  
644 (2021) 109564. doi:10.1016/j.matdes.2021.109564.
- 645 [42] Y. Zhang, M. van de Ven, A. Molenaar, S. Wu, Preventive maintenance of porous asphalt  
646 concrete using surface treatment technology, *Materials & Design*. 99 (2016) 262–272.  
647 doi:10.1016/j.matdes.2016.03.082.
- 648 [43] H. Zhang, K. Anupam, T. Scarpas, C. Kasbergen, S. Erkens, Contact mechanics based solution  
649 to predict modulus of asphalt materials with high porosities, *Materials & Design*. 206 (2021)  
650 109752. doi:10.1016/j.matdes.2021.109752.
- 651 [44] Y. Gu, H. Wang, Y. Yu, Synchronization for commensurate Riemann-Liouville fractional-order  
652 memristor-based neural networks with unknown parameters, *Journal of the Franklin Institute*.  
653 357 (2020) 8870–8898. doi:10.1016/j.jfranklin.2020.06.025.
- 654 [45] H. Li, X. Luo, F. Ma, Y. Zhang, Micromechanics modeling of viscoelastic asphalt-filler  
655 composite system with and without fatigue cracks, *Materials & Design*. 209 (2021) 109983.  
656 doi:10.1016/j.matdes.2021.109983.
- 657 [46] C.F. Lorenzo, T.T. Hartley, Generalized functions for the fractional calculus, National  
658 Aeronautics and Space Administration (NASA), Glenn Research Center, 1999.
- 659 [47] X. Chen, W. Yang, X. Zhang, F. Liu, Unsteady boundary layer flow of viscoelastic MHD fluid  
660 with a double fractional Maxwell model, *Applied Mathematics Letters*. 95 (2019) 143–149.  
661 doi:10.1016/j.aml.2019.03.036  
662